# TAT-RasGAP$_{317-326}$ kills cells by targeting inner-leaflet–enriched phospholipids

Marc Serulla[a], Gabriel Ichim[b,1], Filip Stojceski[c,1], Gianvito Grasso[c], Sergii Afonin[d], Mathieu Heulot[a], Tim Schober[e], Robyn Roth[f], Cédric Godefroy[g], Pierre-Emmanuel Milhiet[g], Kushal Das[h], Ana J. García-Sáez[h], Andrea Danani[c], and Christian Widmann[a,2]

[a]Department of Biomedical Sciences, University of Lausanne, 1005 Lausanne, Switzerland; [b]Center for Research on Cancer of Lyon, LabEX DEVweCAN, University of Lyon, 69008 Lyon, France; [c]Dalle Molle Institute for Artificial Intelligence Research, Università della Svizzera italiana, Scuola Universitaria Professionale della Svizzera Italiana, 6962 Lugano-Viganello, Switzerland; [d]Institute of Biological Interfaces (IBG-2), Karlsruhe Institute of Technology, 76021 Karlsruhe, Germany; [e]Institute of Organic Chemistry, Karlsruhe Institute of Technology, 76131 Karlsruhe, Germany; [f]Washington University Center for Cellular Imaging, Washington University School of Medicine, St. Louis, MO 63110; [g]Centre de Biochimie Structurale, CNRS, INSERM, University Montpellier, 34090 Montpellier, France; and [h]Interfaculty Institute of Biochemistry, Eberhard Karls University Tübingen, 72076 Tübingen, Germany

Edited by John Collier, Harvard Medical School, Boston, MA, and approved October 27, 2020 (received for review July 10, 2020)

**TAT-RasGAP$_{317–326}$ is a cell-penetrating peptide-based construct with anticancer and antimicrobial activities. This peptide kills a subset of cancer cells in a manner that does not involve known programmed cell death pathways. Here we have elucidated the mode of action allowing TAT-RasGAP$_{317–326}$ to kill cells. This peptide binds and disrupts artificial membranes containing lipids typically enriched in the inner leaflet of the plasma membrane, such as phosphatidylinositol-bisphosphate (PIP$_2$) and phosphatidylserine (PS). Decreasing the amounts of PIP$_2$ in cells renders them more resistant to TAT-RasGAP$_{317–326}$, while reducing the ability of cells to repair their plasma membrane makes them more sensitive to the peptide. The W317A TAT-RasGAP$_{317–326}$ point mutant, known to have impaired killing activities, has reduced abilities to bind and permeabilize PIP$_2$- and PS-containing membranes and to translocate through biomembranes, presumably because of a higher propensity to adopt an α-helical state. This work shows that TAT-RasGAP$_{317–326}$ kills cells via a form of necrosis that relies on the physical disruption of the plasma membrane once the peptide targets specific phospholipids found on the cytosolic side of the plasma membrane.**

cell-penetrating peptides | anticancer peptides | membranolytic peptides | phosphatidylserine | phosphoinositides

Most current anticancer therapies trigger genetically encoded regulated cell death pathways to achieve disease control. Manipulation of these pathways can be very efficacious in cancer chemotherapies, as exemplified by the recent development of drugs, such as Venetoclax, that target intrinsic apoptosis-regulating Bcl2 protein family members and that can cure patients suffering from chronic lymphocytic leukemia (1). However, cancer cells, through alterations in cell death pathways, can become refractory to chemotherapeutically induced death leading to relapses (2, 3). Strategies that trigger non-genetically encoded forms of cell death would provide additional therapeutic options to fight cancers.

TAT-RasGAP$_{317–326}$ is a chimeric peptide composed of a cell-penetrating sequence ($G^{48}$RKKRRQRRR$^{57}$) derived from the HIV transactivator of transcription (TAT) protein, and a 10-amino-acid sequence ($W^{317}$MWVTNLRTD$^{326}$) derived from the Src homology 3 domain of p120 RasGAP (Ras GTPase-activating protein) (4). This construct has several anticancer properties, including inhibition of metastatic progression and tumor cell sensitization to anticancer therapies (4–6). This peptide also displays broad antimicrobial activities (7).

The first reported anticancer activity of TAT-RasGAP$_{317–326}$ was its ability to sensitize tumor cells, but not normal cells, to genotoxin-induced death (4) and to radiotherapy (8). Based on these findings, the peptide was tested in preclinical animal models and was shown to sensitize tumor xenografts in mice to cisplatin, doxorubicin, and ionizing radiation with no apparent toxicity to healthy tissues (8, 9). Even though TAT-RasGAP$_{317–326}$ injected intraperitoneally can reach and sensitize tumors located subcutaneously, it is, like other cell-penetrating peptides (10), rapidly cleared from the organism (8). This may compromise its use as a systemic agent (7). Hence, future clinical development of TAT-RasGAP$_{317–326}$ will probably be in the direction of topical or on-target use.

In addition to sensitizing tumors to an anticancer regimen, TAT-RasGAP$_{317–326}$ can also directly kill a subset of cancer cell lines in a manner that is distinct from apoptosis, necroptosis, parthanatos, pyroptosis, and autophagy (7). This peptide appears, therefore, to harbor killing properties that may be difficult for cancer cells to alleviate through resistance-building alterations within known regulated cell death pathways. A single point mutation in the RasGAP moiety (W317A) abrogates all of the anticancer and antimicrobial properties of the peptide (7, 11, 12). The mechanisms used by TAT-RasGAP$_{317–326}$ to kill cells have eluded detailed characterization until now. In the present study, we provide experimental evidence that this peptide induces a necrotic-like form of death by targeting phospholipids enriched in the inner leaflet of the plasma membrane.

## Results

**TAT-RasGAP$_{317–326}$ Needs to Access the Cytoplasm to Kill Cells.** We have recently demonstrated that TAT-RasGAP$_{317–326}$ accesses the cytoplasm through direct translocation across the plasma

### Significance

TAT-RasGAP$_{317–326}$ can lyse cancer cells in a manner distinct from known programmed cell death pathways through its ability to target specific plasma membrane lipids. The killing properties of this peptide may therefore be difficult for cancer cells to alleviate through resistance-building alterations within known regulated cell death pathways. TAT-RasGAP$_{317–326}$ and compounds with similar anticancer activities can potentially complement existing anticancer therapies based on the use of genotoxins or radiation that induce apoptosis.

Author contributions: M.S., G.G., S.A., P.-E.M., A.J.G.-S., A.D., and C.W. designed research; M.S., G.I., F.S., G.G., S.A., M.H., T.S., R.R., C.G., and K.D. performed research; K.D. contributed new reagents/analytic tools; M.S., G.I., F.S., G.G., S.A., A.D., and C.W. analyzed data; and M.S. and C.W. wrote the paper.

The authors declare no competing interest.

This article is a PNAS Direct Submission.



[1]G.I. and F.S. contributed equally to this work.

[2]To whom correspondence may be addressed. Email: christian.widmann@unil.ch.

This article contains supporting information online at https://www.pnas.org/lookup/suppl/doi:10.1073/pnas.2014108117/-/DCSupplemental.

membrane in a membrane-potential–dependent manner (13). Direct translocation of TAT-RasGAP$_{317–326}$ and other cationic cell-penetrating peptides can be prevented by membrane-depolarizing agents such as gramicidin or extracellular high-potassium concentrations (13, 14). Depolarizing cells with 100 mM extracellular KCl does not affect, or only minimally affects, at higher peptide concentrations, the initial cell-surface binding of TAT-RasGAP$_{317–326}$ (*SI Appendix*, Fig. S1*A*). Depolarization, however, does decrease the ability of the cells to take up the peptide by a factor of about 100 (*SI Appendix*, Fig. S1*B*, *Upper*) and fully prevents the peptide from killing cells (*SI Appendix*, Fig. S1*B*, *Lower*). The residual peptide uptake in depolarized cells corresponds to the endocytosis of peptides that remain trapped in endosomes (*SI Appendix*, Fig. S1*C*) (13).

**Preferential Binding of TAT-RasGAP$_{317–326}$ to Inner-Leaflet Phospholipids.** Several anticancer peptides possess membranolytic activity (15–17). To assess if TAT-RasGAP$_{317–326}$ has a specific selectivity for individual plasma membrane phospholipids, multilamellar vesicles (MLVs) made of various phospholipid compositions were incubated with a fluorescent version of the peptide. As negative controls, the TAT-RasGAP$_{317–326}$ W317A substitution mutant was used, as well as the TAT cell-penetrating peptide alone. Replacing the first tryptophan residue (W317) in TAT-RasGAP$_{317–326}$ with an alanine residue hampers all of the known cellular activities of the peptide (11, 12). This mutation does not prevent the peptide from accessing the cytosol (*SI Appendix*, Fig. S2*A*), even though quantitatively the extent of cellular uptake was found to be lower for the W317A mutant compared to the wild-type peptide (*SI Appendix*, Fig. S2*B*). In conditions of similar uptake (*SI Appendix*, Fig. S2*C*), the mutant peptide was far less potent in killing cells compared to the wild-type peptide (*SI Appendix*, Fig. S2*D*). In short-term incubation settings, the W317A mutant peptide was unable to induce cell death (*SI Appendix*, Fig. S2*E*).

The lipids used in this study are listed in *SI Appendix*, Table S1. *SI Appendix*, Table S2, provides the composition of the cytosolic ("inner") and extracellular ("outer") leaflets of the plasma membrane that we have considered in the present work. Fig. 1*A* shows that TAT-RasGAP$_{317–326}$ and control peptides do not bind to liposomes made of lipids present on both sides of the plasma membrane such as phosphatidylcholine (PC), phosphatidylethanolamine (PE), or cholesterol. Similar results were obtained when these peptides were incubated with lipids typically present in the outer leaflet of the plasma membrane like GM1 and GM3 gangliosides or sphingomyelin (SM). On the other hand, TAT-RasGAP$_{317–326}$ bound to inner-leaflet–enriched phosphatidylinositol(4,5)bisphosphate (PI[4,5]P$_2$) and phosphatidylserine (PS) more avidly than control peptides. Binding equilibrium between the peptides and PS (20%)-containing liposomes was reached after 15 min of incubation (*SI Appendix*, Fig. S3). Other lipids present in the inner leaflet of the plasma membrane either did not interact with TAT-RasGAP$_{317–326}$ (e.g., phosphatidylinositol) or displayed no specificity for the wild-type peptide (e.g., phosphatidic acid). Cardiolipin, a mitochondria-specific phospholipid, when present at a 10% concentration in liposomes, interacted more strongly with TAT-RasGAP$_{317–326}$ compared to the control peptides. The specificity of this binding was lost when the level of cardiolipin in liposomes rose to 20%, which is the physiological concentration of this lipid in the inner mitochondrial membrane. TAT-RasGAP$_{317–326}$ had a much higher affinity for vesicles, the lipid composition of which mimicked the inner-leaflet plasma membrane compared to bilayers made of outer-leaflet membrane-specific lipids. TAT-RasGAP$_{317–326}$ displayed a specific propensity to bind bisphosphorylated phosphoinositides, such as PI(4,5)P$_2$ and PI(3,5)P$_2$, and, to a lower extent, PI(3,4)P$_2$. Monophosphate phosphoinositides like PI(3)P interacted very poorly with the peptides. There was no specific binding of the wild-type peptide to PI(3,4,5)P$_3$. We also note that, in almost all cases, the W317A mutant demonstrated binding preferences similar to the TAT-only control, suggesting a more substantial impact of the RasGAP moiety of TAT-RasGAP$_{317–326}$, rather than its TAT part, in the binding-specifying peptide–lipid interactions.

Lipid-binding preferences were also tested with unlabeled peptides using membranes spotted with different lipids (Fig. 1*B*). PI(4)P was bound by all peptides, including TAT alone. Phosphatidic acid was bound by both TAT-RasGAP$_{317–326}$ and the W317A mutant. The lipids specifically recognized by TAT-RasGAP$_{317–326}$ but not by the other peptides were cardiolipin, PI(4,5)P$_2$, PS, and, to a lower extent, PI(3,4,5)P$_3$. These data confirm the binding preferences of TAT-RasGAP$_{317–326}$ for cardiolipin and lipids enriched in the cytoplasmic side of the plasma membrane.

**TAT-RasGAP$_{317–326}$ Kills Cells in a Mitochondria-Independent Manner.** The observation that TAT-RasGAP$_{317–326}$ displays high affinity to cardiolipin suggests a mitochondria involvement in the peptide-mediated cell death. To determine if binding to cardiolipin underlies the ability of the peptide to permeabilize membranes, giant unilamellar vesicles (GUVs) containing cardiolipin were incubated with TAT-RasGAP$_{317–326}$ and control peptides. The membrane integrity was then evaluated through calcein intake. GUVs containing 10% cardiolipin, the concentration at which specificity of binding of the wild-type peptide versus the control peptides was observed (Fig. 1), were not markedly permeabilized by TAT-RasGAP$_{317–326}$ (Fig. 2*A*). Even though high-cardiolipin-concentration (20%)–containing vesicles could be permeabilized by wild-type TAT-RasGAP$_{317–326}$ to some extent (*SI Appendix*, Fig. S4), it appears that cardiolipin is, in fact, a rather protective phospholipid against permeabilization. Indeed, PC-containing vesicles are less lysed by high concentrations of TAT-RasGAP$_{317–326}$ when they contain cardiolipin (compare Figs. S4 and S5 in *SI Appendix*). Removing mitochondria from HeLa cells (Fig. 2 *B* and *C*), while preventing mitochondria-dependent cell death, did not render them resistant to TAT-RasGAP$_{317–326}$–induced death (Fig. 2*D*). Hence, even though the peptide can bind to cardiolipin-containing membranes, this interaction does not appear to mediate the ability of the peptide to kill cells.

**TAT-RasGAP$_{317–326}$ Permeabilizes Membranes Made of Inner-Leaflet Phospholipids.** As shown above, TAT-RasGAP$_{317–326}$ preferentially binds phospholipids enriched in the inner leaflet of the plasma membrane, such as phosphatidylserine and bisphosphorylated phosphoinositides. GUVs containing either PI(4,5)P$_2$ or PS were efficiently permeabilized by TAT-RasGAP$_{317–326}$ but not (in the case of PS) or inefficiently (in the case of PI[4,5]P$_2$) by the mutant W317A peptide (Fig. 3). Similar results were obtained with other bisphosphorylated phosphoinositides such as PI(3,4)P$_2$ and PI(3,5)P$_2$ (*SI Appendix*, Fig. S6). Permeabilization was generally accompanied by accumulation of lipid material (micelles) outside GUVs, an indication of a detergent-like effect (18). GUVs with outer-membrane–like composition were not significantly permeabilized by the peptides (Fig. 3). In contrast, GUVs made of inner-membrane–enriched phospholipids were very efficiently permeabilized by TAT-RasGAP$_{317–326}$. The control TAT-RasGAP$_{317–326}$(W317A) peptide was about 10-fold less efficient in permeabilizing these GUVs compared to the wild-type peptide (Fig. 3).

To further evaluate the mode of permeabilization induced by TAT-RasGAP$_{317–326}$, we performed electron microscopy (EM) visualization of HeLa cells incubated with the peptide. Cells experienced gross membrane disruption upon peptide addition without any indication of pore formation such as seen upon addition of the streptolysin O hemolytic exotoxin (*SI Appendix*, Fig. S7). Although we cannot exclude that the peptide creates

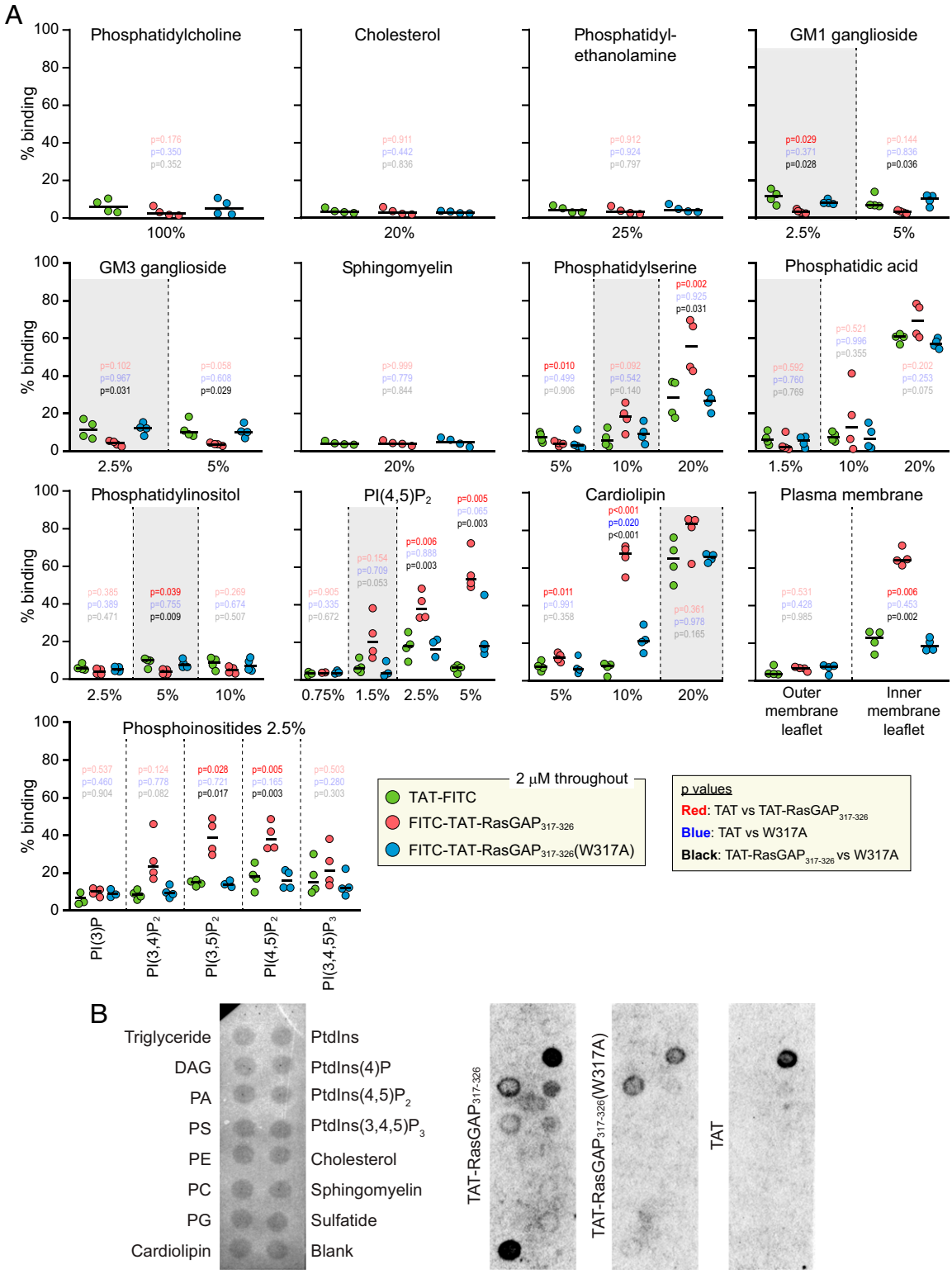


**Fig. 1.** Preferential binding of TAT-RasGAP$_{317–326}$ to inner-leaflet phospholipids. (*A*) MLVs were generated with the indicated percentages of the specified lipids in the figure (the remaining lipid being phosphatidylcholine). Outer-leaflet liposomes contained PC 64.4%, PE 10.6%, SM 20%, GM1 2.5%, and GM3 2.5% while inner-leaflet liposomes contained PC 51.25%, PE 36.25%, PS 10%, and PI(4,5)$P_2$ 2.5%. Liposomes were incubated 30 min with 2 μM of FITC-labeled versions of TAT, TAT-RasGAP$_{317–326}$, and TAT-RasGAP$_{317–326}$(W317A). Binding of these peptides to liposomes was then determined ($n = 4$). The zones highlighted in light gray correspond to the physiological concentrations found in plasma membranes. Statistical analysis was performed using one-way ANOVA with Geisser–Greenhouse correction (sphericity not assumed), followed by post-hoc Tukey multicomparison tests between means of all groups. (*B*) Membranes spotted with the indicated lipids were incubated with 0.5 mg/mL TAT-RasGAP$_{317–326}$, TAT-RasGAP$_{317–326}$(W317A), and TAT for 1 h, and the interaction with the lipid was revealed by immunoblotting using an anti-TAT antibody. Blots are representative of two independent experiments.

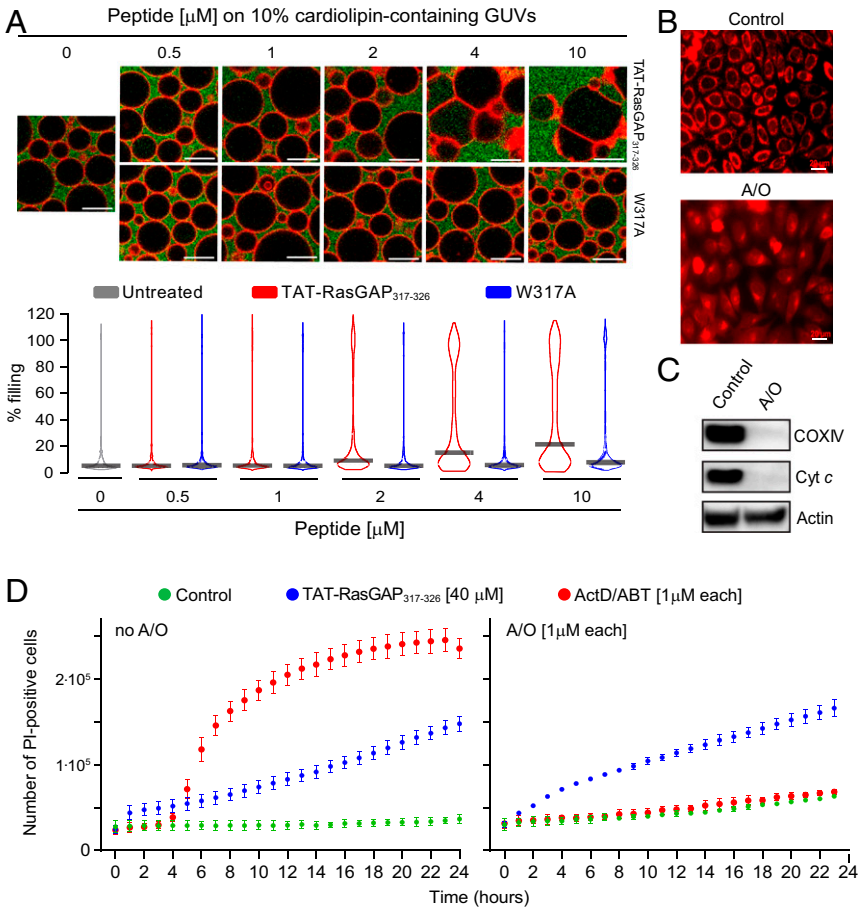


**Fig. 2.** TAT-RasGAP$_{317–326}$ kills HeLa cells in a mitochondria-independent manner. (*A*) GUVs containing 10% cardiolipin were incubated or not for 1 h with TAT-RasGAP$_{317–326}$ or TAT-RasGAP$_{317–326}$(W317A) at the indicated concentrations. GUV permeabilization was evaluated by calcein uptake using confocal microscopy. Representative images are presented. (Scale bar, 10 μm.) Quantitation is shown as violin plots (dark-gray bars indicate the median). (*B* and *C*) Mitochondria in HeLa cells stably expressing YFP-Parkin were removed by enforced mitophagy followed by a 36-h incubation with 1 μM antimycin A and 1 μM oligomycin (A/O) or vehicle (ethanol 0.2%) (Control). Antimycin A (an inhibitor of ubiquinone oxidation in the cytochrome *c* oxidase complex) and oligomycin (an ATP synthase inhibitor) are compounds that disrupt mitochondrial function and trigger Parkin-mediated complete mitophagy. The presence of mitochondria was assessed with the MitoTracker Red CMXRos dye (*B*). (Scale bar, 20 μm.) In healthy cells, the mitotracker dye specifically stains the mitochondrial network, while in cells undergoing complete mitophagy the cytoplasmic signal is strongly reduced and appears diffused. Alternatively, the expression of cytochrome *c* (Cyt *c*), cytochrome *c* oxidase (COX IV), and actin in these cells was assessed by Western blot analysis (*C*). (*D*) HeLa cells ectopically expressing YFP-Parkin were treated as in *B* and *C*. These cells were then incubated with the indicated compounds for various periods of time (ActD, actinomycin D; ABT, ABT737). ActD is a transcription inhibitor, and ABT737 is an antiapoptotic Bcl-2 family protein antagonist. The combination of these two drugs induces rapid cell death via the intrinsic (i.e., mitochondria-dependent) apoptotic pathway. Cell death was assessed using a live-cell imaging system (*Materials and Methods*). Results are expressed as the mean ± SD of three biologically independent experiments.

small and/or transient pores that escape detection by EM, these data are consistent with the notion that TAT-RasGAP$_{317–326}$ disrupts cellular membranes in a detergent-like manner.

**PI(4,5)P$_2$ Plasma Membrane Depletion Impairs TAT-RasGAP$_{317–326}$–Induced Cell Death.** Lipid binding and GUV permeabilization experiments indicate that TAT-RasGAP$_{317–326}$ induces cell death by direct permeabilization of the plasma membrane through binding to phospholipids like PI(4,5)P$_2$. Depleting this phospholipid from the inner layer of the plasma membrane should therefore hamper TAT-RasGAP$_{317–326}$ from killing cells. We tested this assumption by inducing the translocation to the plasma membrane of an enzyme able to dephosphorylate the inositol ring of phosphoinositides at position 5 (Fig. 4 *A* and *B*), thereby diminishing the levels of PI(4,5)P$_2$ as assessed by decreased recruitment of PI(4,5)P$_2$-binding proteins to the plasma membrane (Fig. 4*C*). This treatment lowered the ability of the peptide to permeabilize cells (Fig. 4*D*) without affecting its uptake (Fig. 4*E*).

**TAT-RasGAP$_{317–326}$ Membranolytic Activity Is Antagonized by the Endosomal Sorting Complex Required for Transport Machinery.** Plasma membrane damage triggers a healing response through removal of damaged areas by endocytosis or via exosome shedding. The endosomal sorting complex required for transport (ESCRT) machinery has recently been shown to participate in such membrane repair events (19, 20). If TAT-RasGAP$_{317–326}$ has membranolytic activities through its ability to target inner-leaflet phospholipids as indicated by the results shown above, it can be foreseen that the ESCRT machinery antagonizes the killing activity of the peptide. To assess this hypothesis, dominant-negative CHMP3$_{1–179}$ and VPS4A$^{E228Q}$, core members of the ESCRTIII complex, and the ESCRT disassembly subcomplex, respectively, were expressed in HeLa cells using a doxycycline-inducible system (Fig. 5*A*). This manipulation sensitized cells to TAT-RasGAP$_{317–326}$–induced death (Fig. 5*B*). In the case of CHMP3$_{1–179}$, the sensitization could be partly explained by an increase in peptide uptake (Fig. 5*C*, *Middle*). However,

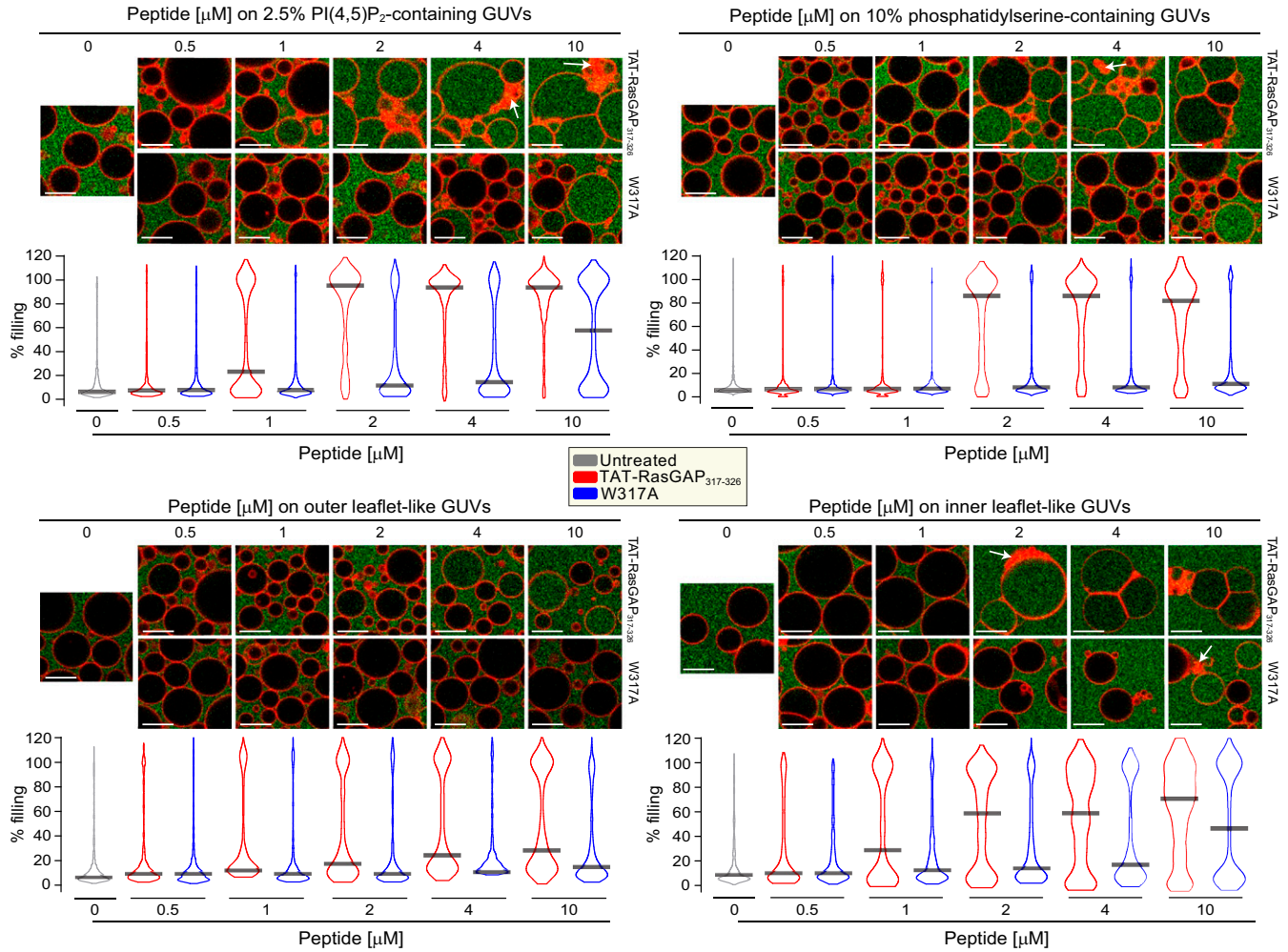


**Fig. 3.** TAT-RasGAP$_{317–326}$ permeabilizes membranes made of inner-leaflet phospholipids. GUVs made of lipid mixtures mimicking the outer-leaflet (PC 64.4%, PE 10.6%, SM 20%, GM1 2.5%, GM3 2.5%) or inner-leaflet (PC 51.25%, PE 36.25%, PS 10%, PI(4.5)$P_2$ 2.5%) plasma membrane composition and GUVs containing 2.5% PI(4,5)$P_2$ (and 97.5% PC) or 10% PS (and 90% PC) were treated or not for 1 h with TAT-RasGAP$_{317–326}$ or TAT-RasGAP$_{317–326}$(W317A) at the indicated concentrations. GUV permeabilization was evaluated by calcein intake using confocal microscopy. Representative images are presented. (Scale bar, 10 μm.) Quantitation is shown as violin plots (median is indicated by a dark-gray bar). See *SI Appendix*, Table S1, for lipid abbreviations. Arrows point to accumulation of lipid material (micelles) outside GUVs.

VPS4A$^{E228Q}$ expression in cells did not affect peptide uptake (Fig. 5*C*, *Right*) while still protecting cells from TAT-RasGAP$_{317–326}$ (Fig. 5*B*, *Right*). These data therefore indicate that the ESCRT machinery repairs TAT-RasGAP$_{317–326}$–induced membrane damage and protects cells from the peptide's lytic activity.

**Peptide Uptake Efficiency or Internal PS Levels by Themselves Do Not Explain the Sensitivity to TAT-RasGAP$_{317–326}$–Induced Cell Death.** Even though there is variability in terms of their sensitivity to TAT-RasGAP$_{317–326}$–induced death, tumor cells are more efficiently killed by the peptide than are nontransformed cells (12). The sensitivity to TAT-RasGAP$_{317–326}$ has been reported to be unrelated to the mutation status of tumor cell lines, and there is no indication that expression of certain genes is specifically associated with TAT-RasGAP$_{317–326}$ sensitivity (12). Here we aimed to determine whether the susceptibility of a panel of six tumor cell lines to be killed by TAT-RasGAP$_{317–326}$ was related to their capacity to take up the peptide or to their intracellular PS levels. *SI Appendix*, Fig. S8*A*, shows that the panel could be divided in two groups based on the sensitivity of the cell lines to the peptide. In the sensitive group (U2OS, Raji, and SKW6.4), half of the cells were killed by ~20 μM TAT-RasGAP$_{317–326}$, while in the less sensitive group (HeLa, Chinese hamster ovary, and human embryonic kidney 293T cells), more than 40 μM of the peptide was required to kill half of the cell population. The cells that displayed the highest ability to acquire the peptide were those of the sensitive group with the exception of U2OS (*SI Appendix*, Fig. S8*B*). To test if levels of PS in cells correlated with the sensitivity to TAT-RasGAP$_{317–326}$–induced death, intracellular PS levels were measured in fully permeabilized cells (*SI Appendix*, Fig. S8*C*) using saturating Annexin V levels (*SI Appendix*, Fig. S8*D*). Cell lines with the highest intracellular levels were found in the sensitive group (*SI Appendix*, Fig. S8*E*), again with the exception of U2OS cells. In the absence of a strict correlation between the tested factors and TAT-RasGAP$_{317–326}$ sensitivity, one has to conclude that the ability of cells to be killed by TAT-RasGAP$_{317–326}$ is likely determined by a combination of factors that can include those tested here but that in isolation are not sufficient to explain the susceptibility of a given cell type to the peptide.

**The W317A Substitution, but Not the W317F Substitution, Promotes Helicity in RasGAP$_{317–326}$, Affecting Peptide–Membrane Interaction.** To assess if the diminished specific lipid-binding capacity of W317A results from a secondary structure distinct from the one adopted by TAT-RasGAP$_{317–326}$, the peptide structures and

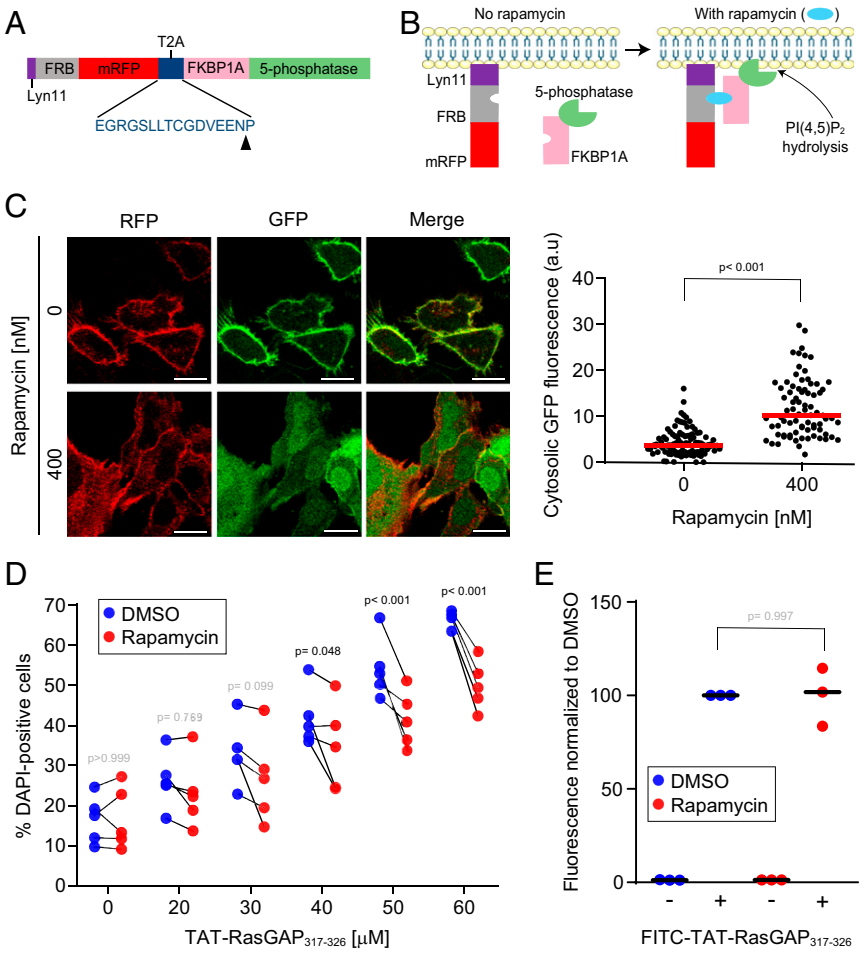


**Fig. 4.** PI(4,5)$P_2$ plasma membrane depletion impairs TAT-RasGAP$_{317–326}$–induced cell death. (*A*) Schematic description of the plasmid (hLyn[1-11]-hMTOR [2021-2113]-HA-mRFP-T2A-hFKBP1A-Inp54p) encoding the protein constructs allowing rapamycin-controlled PI(4,5)$P_2$ dephosphorylation. This plasmid contains an open reading frame encoding two proteins separated by a self-cleaving T2A peptide (32), the sequence of which is shown in blue with the cleavage site indicated by an arrowhead. The first protein corresponds to a fusion protein between the monomeric red fluorescent protein (mRFP) and the FKBP rapamycin binding (FRB) domain of human mammalian target of rapamycin. This fusion protein is tagged at the N terminus with the first 11 amino acids of human Lyn that allows plasma membrane targeting via myristoylation and palmitoylation (33). An HA tag is located between FRB and mRFP (not shown in the figure). The second protein is a fusion protein between Inp54p, a yeast phosphatidylinositol-4,5-bisphosphate 5-phosphatase (34) and the human FK506-binding protein FKBP1A (also known as FKBP12). (*B*) Scheme depicting the principle of the procedure allowing PI(4,5)$P_2$ depletion at the plasma membrane level. In the presence of rapamycin, FRB and FKBP12 dimerize, resulting in plasma membrane targeting of Inp54p. *A* and *B* were adapted from ref. 35. (*C*) HeLa cells were transiently transfected (at a 3:1 ratio) with the construct depicted in *A* and PH-PLCD1[1-170]-GFP, a plasmid encoding a fusion protein between GFP and the pleckstrin homology (PH) domain of PLCδ1. This PH domain binds to PI(4,5)$P_2$ and functions as a PI(4,5)$P_2$ localization biosensor in cells. The transfected cells were treated for 1 h with rapamycin (400 nM) or vehicle (0.2% dimethylsulfoxide [DMSO]) and then were subjected to live imaging using confocal microscopy. (Scale bar, 20 μm.) Cytosolic GFP fluorescence was quantitated as indicated in *Materials and Methods*. Dots correspond to individual cells. Medians are indicated by red bars. (*D*) HeLa cells were transiently transfected with the construct depicted in *A*. The cells were then pretreated for 1 h with 400 nM of rapamycin or vehicle (0.2% DMSO), followed by 6 h of incubation with the indicated concentrations of TAT-RasGAP$_{317–326}$. Plasma membrane permeabilization was tested by DAPI staining and measured by flow cytometry in mRFP-positive cells. (*E*) Alternatively, following the rapamycin treatment, the cells were subjected to 1 h of incubation with 20 μM FITC-labeled TAT-RasGAP$_{317–326}$. Peptide uptake was evaluated in mRFP-positive cells by flow cytometry. FITC fluorescence was normalized against the "DMSO + peptide" condition. Statistical analysis was performed using paired *t* test (*C* and *E*) or two-way ANOVAs followed by post hoc Sidak's multicomparison test with matched comparison (*D*). In *D* and *E*, each point represents an individual experiment, and the horizontal black bar in *E* corresponds to the median. In *D*, values from a given independent experiment are connected with thin black lines.

peptide–membrane interactions were studied by molecular modeling, circular dichroism (CD), and solid-state NMR spectroscopy (ssNMR). Simulation experiments were performed with TAT-RasGAP$_{317–326}$ and the W317A mutant in the presence of lipid bilayers of variable compositions. The in silico experiments were performed using atomistic unbiased simulations in order to study the peptides interfacial interactions with phospholipidic bilayers (21) and how the latter influence the conformational transitions of the peptides. In the membrane-bound states, the propensity of TAT-RasGAP$_{317–326}$ to adopt an α-helical structure within the RasGAP moiety was very low, in sharp contrast to the W317A mutant, regardless of the lipid composition of the model bilayers (Fig. 6). The observed helicity of the TAT moiety was barely affected by the W317A mutation. This indicates that a tryptophan at position 317 is a potent α-helix disruptor within the RasGAP sequence of TAT-RasGAP$_{317–326}$.

The different conformations of the two bound peptides translated into differential, but still lipid composition-independent, modes of membrane insertion (Fig. 7). The less structured wild-type peptide was found to insert slightly deeper into membranes compared to the W317A mutant (Fig. 7*A*). This was due to a higher likelihood of amino acids around the W317

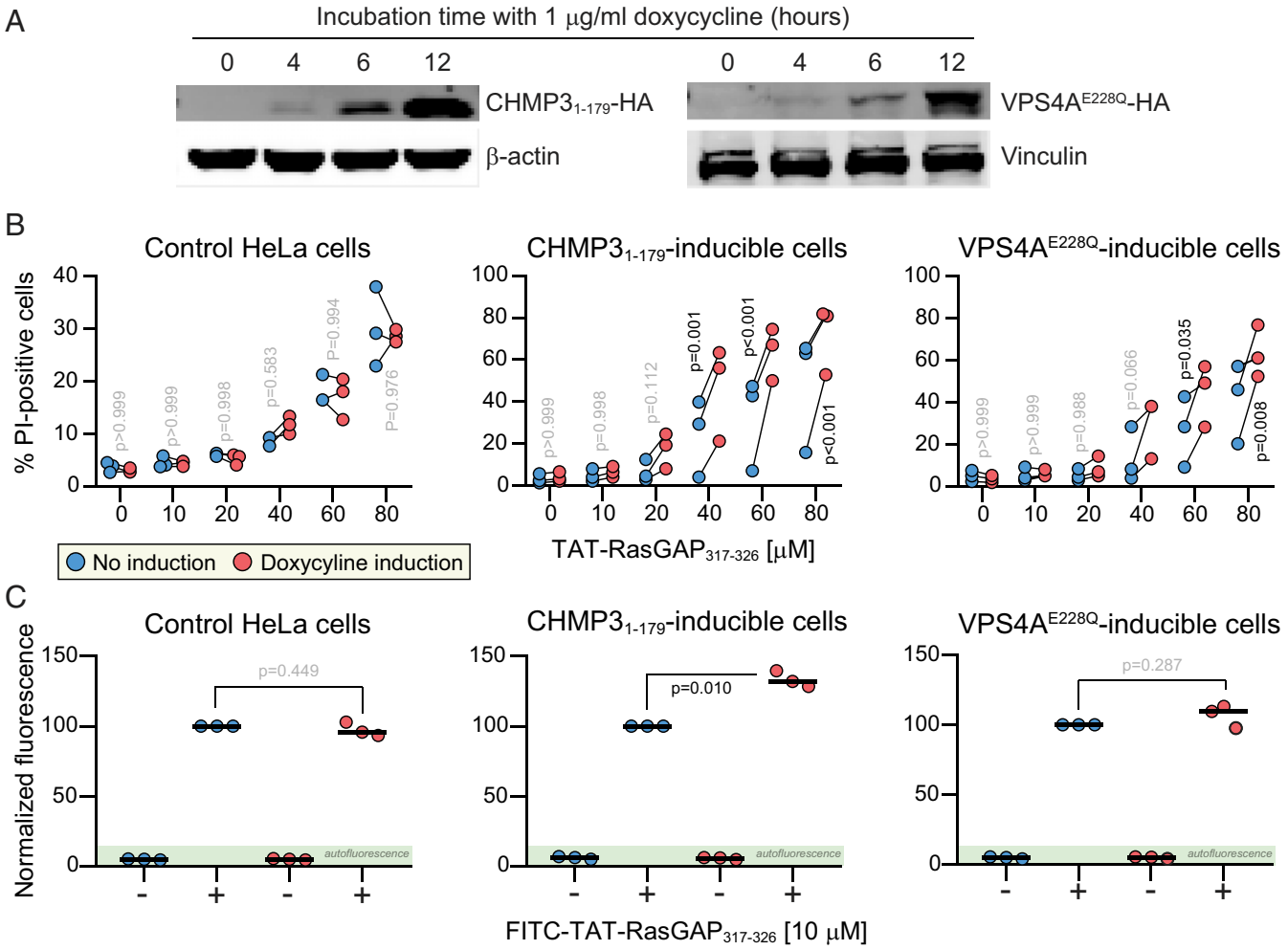


**Fig. 5.** Dominant-negative mutants of the ESCRT machinery sensitize cells to TAT-RasGAP$_{317–326}$–induced death. (*A*) HeLa cells expressing the doxycycline-inducible HA-tagged CHMP3$_{1–179}$ and VPS4A$^{E228Q}$ constructs were treated with doxycycline for the indicated periods of time. Expression of the tagged proteins was assessed by Western blot. Vinculin and β-actin were used as loading controls (vinculin was used for VPS4A$^{E228Q}$-inducible cells as β-actin and VPS4A have similar apparent molecular weight). (*B*) Control HeLa cells and the HeLa clones described in *A* were stimulated for 6 h in the presence or in the absence of doxycycline and then incubated, still in the presence of doxycycline, with the indicated concentrations of TAT-RasGAP$_{317–326}$ for 6 additional hours. Plasma membrane damage was tested by flow cytometry after PI staining. Values from a given independent experiment are connected with thin black lines. (*C*) Alternatively, after the doxycycline stimulation, cells were incubated with a sublethal concentration (10 μM) of FITC-labeled TAT-RasGAP$_{317–326}$ for 1 h. Peptide uptake was measured by flow cytometry. Fluorescence from the plasma membrane-attached peptide was quenched with 0.2% Trypan blue. The data were normalized against the "noninduced + peptide" condition. Two-way ANOVAs followed by post hoc Sidak's multicomparison test with matched comparison (*B*) and paired *t* test (*C*) were used to assess the significance of the observed differences.

residue to contact lipids of the inner-leaflet–like membrane (Fig. 7*B*). Furthermore, the TAT segment of the wild-type peptide appeared to "attack" the membrane with a sharper angle than the W317A mutant (Fig. 7*C*) but without significant modulation of the overall probability to contact the lipids (Fig. 7*B*).

Circular dichroism experiments, comparing the conformations of the wild-type and the W317A peptides in the presence of membrane mimetics, provided additional evidence that the W317A mutation impacts the peptide's conformation. At identical concentrations, we observed more intense CD signals or more pronounced spectral features associated with folding for the W317A peptide. For example, in the helix-promoting TFE (2,2,2-trifluoroethanol) the mutant peptide showed a more typical α-helix since 1) its $\pi\rightarrow\pi^*$ parallel transition (*SI Appendix*, Fig. S9*A*) occurred close to the canonical 208-nm wavelength while the wild-type peptide displayed a slightly left (blue)-shifted $\pi\rightarrow\pi^*$ parallel transition (*SI Appendix*, Fig. S9*B*) and 2) the amplitude of the PE and phosphatidic acid signals (*SI Appendix*, Fig. S9*A*) registered with the W317A mutant were considerably larger than those of the parental peptide (*SI Appendix*, Fig. S9*B*). While the W317A substitution favored helicity, it did not affect the overall peptide conformational plasticity. Indeed, the spectra of TAT-RasGAP$_{317–326}$ and its W317A mutant were similar in aqueous or 1:1 TFE:PB (phosphate buffer) environments, as well as in the presence of the zwitterionic detergent dodecylphosphocholine or in negatively charged *lyso*-phosphatidylglycerol micelles (*SI Appendix*, Fig. S9*B*). Finally, in negatively charged dodecylsulfate micelles, TAT-RasGAP$_{317–326}$ folded to a more extended conformation as judged by the pronounced negative band at 196 nm and the strong positive signal around 225 nm. This indicates a turn-like geometry contribution since the $n\rightarrow\pi^*$ transition occurred red-shifted (>220 nm) instead of at the 217 to 218 nm wavelength seen for classical β-strand. A propensity of the peptides to assume continuous secondary-structure–breaking backbone turn(s) or kink(s) is further corroborated by the presence of

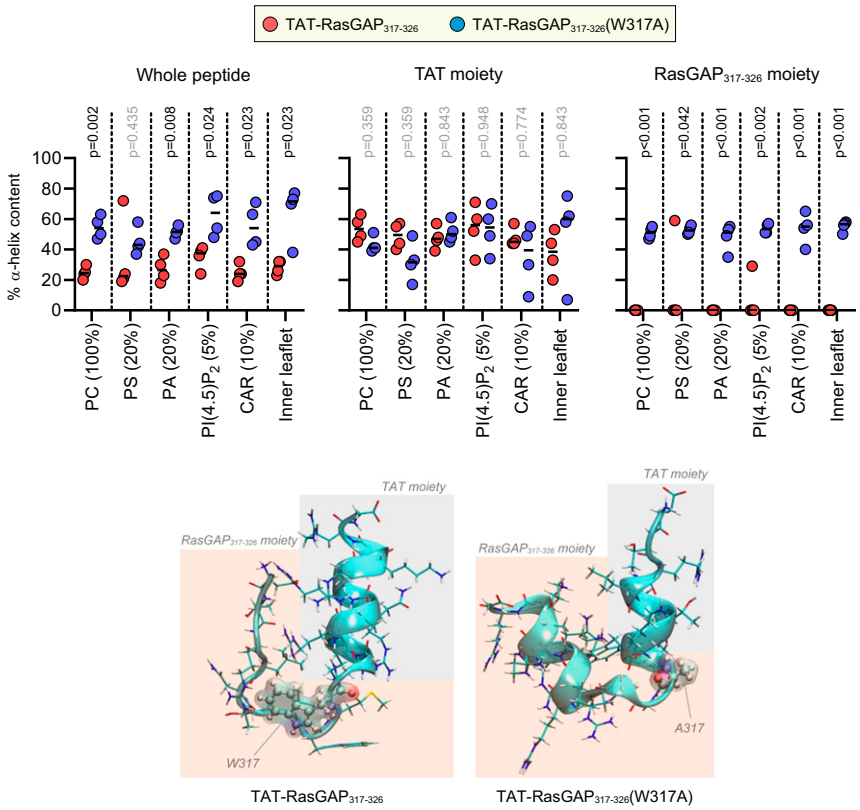


**Fig. 6.** The W317A mutation promotes alpha helix formation in the RasGAP moiety of TAT-RasGAP$_{317–326}$. The secondary structure of TAT-RasGAP$_{317–326}$ in the presence of the indicated membrane lipid environment was assessed by in silico simulations as described in the methods (four simulations per condition). The membrane compositions are presented in *SI Appendix*, Table S3. The graph depicts the α-helicity content in the whole TAT-RasGAP$_{317–326}$ peptide as well as in its individual TAT and RasGAP$_{317–326}$ moieties. The median is indicated by black bars. Paired *t* tests were used to assess statistical significance. The structures presented below the graphs are snapshot examples of the structures obtained for TAT-RasGAP$_{317–326}$ and its W317A mutant at the beginning of molecular dynamics simulations, i.e., before the peptides interact with membranes.

a dispersive feature around 225 nm. The latter is more pronounced for the wild-type peptide, e.g., in PB and in the presence of lyso-phosphatidylcholine. This correlates with the expected higher rigidity of the backbone around tryptophan residue in this sequence and resembles the CD signals often observed in tryptophan-containing small cyclic peptides (22–25).

Negative curvature may facilitate peptide translocation through membrane (26), while positive curvature may trigger lipid-packing defects and membrane disruption (27). We used $^{31}$P ssNMR to investigate potential differences between TAT-RasGAP$_{317–326}$ and its W317A mutant in membrane curvature modulation. Specifically, we studied the temperatures ($T_{L-H}$) at which lamellar (L) to inverted hexagonal ($H_{II}$) lipid-phase transition (*SI Appendix*, Fig. S10*A*) occurred in PE-based membranes reconstituted with the two peptides (*SI Appendix*, Fig. S10*B*). In pure PE membranes, TAT-RasGAP$_{317–326}$ promoted negative curvature since the $H_{II}$ phase was already detected at the lowest tested temperature (5 °C). The L-to-$H_{II}$ phase transition nominally occurs between 15° and 20° in untreated membranes. In contrast, the W317A mutant peptide favored positive curvature (*SI Appendix*, Fig. S10*B*). As the outer membrane leaflet is globally composed of neutral phospholipids, as in the model PE bilayer used here, this could mechanistically explain the reduced ability of the W317A mutant to enter cells (*SI Appendix*, Fig. S2). In PE membranes loaded with negatively charged lipids (PS and PG), an environment closer to what is found in the inner layer of the plasma membrane, the wild-type peptide lost its negative-membrane–curving abilities and gained positive-membrane–curving properties (*SI Appendix*, Fig. S10*B*). The increased propensity to induce positive membrane curvature on inner-layer–like membranes may be part of the mechanism used by TAT-RasGAP$_{317–326}$ to destabilize membranes. The difference in L-to-$H_{II}$ phase-transition–inducing properties observed between the two peptides in PE membranes disappeared upon addition of anionic lipids. This is compatible with the notion that TAT-RasGAP$_{317–326}$ ended up more concentrated than its mutant in the vicinity of the membrane due to stronger affinities for negatively charged phospholipids (Fig. 1).

Finally, we tested if α-helix disruption in RasGAP$_{317–326}$ allowing TAT-RasGAP$_{317–326}$ to permeabilize cells was exclusive of tryptophan at position 317 or other aromatic amino acids could act in a similar way. TAT-RasGAP$_{317–326}$(W317F) preserved the ability of TAT-RasGAP$_{317–326}$ to kill cells (*SI Appendix*, Fig. S11*A*) and to disrupt α-helix formation in the RasGAP$_{317–326}$ moiety (*SI Appendix*, Fig. S11*B*). One could argue that the W317A but not the W317F substitution diminishes TAT-RasGAP$_{317–326}$ hydrophobicity and that this affects TAT-RasGAP$_{317–326}$ membranolytic activity. However, no significant hydrophobicity differences were observed between the wild-type and mutant peptides (*SI Appendix*, Fig. S11*C*).

## Discussion

TAT-RasGAP$_{317–326}$ has been reported earlier to kill cells using a nonregulated necrotic-like death pathway (12). The present work provides the molecular characterization of this pathway, which is schematically described in *SI Appendix*, Fig. S12. TAT-RasGAP$_{317–326}$ needs to enter cells by direct translocation through the plasma membrane to exert its biological activity (*SI*

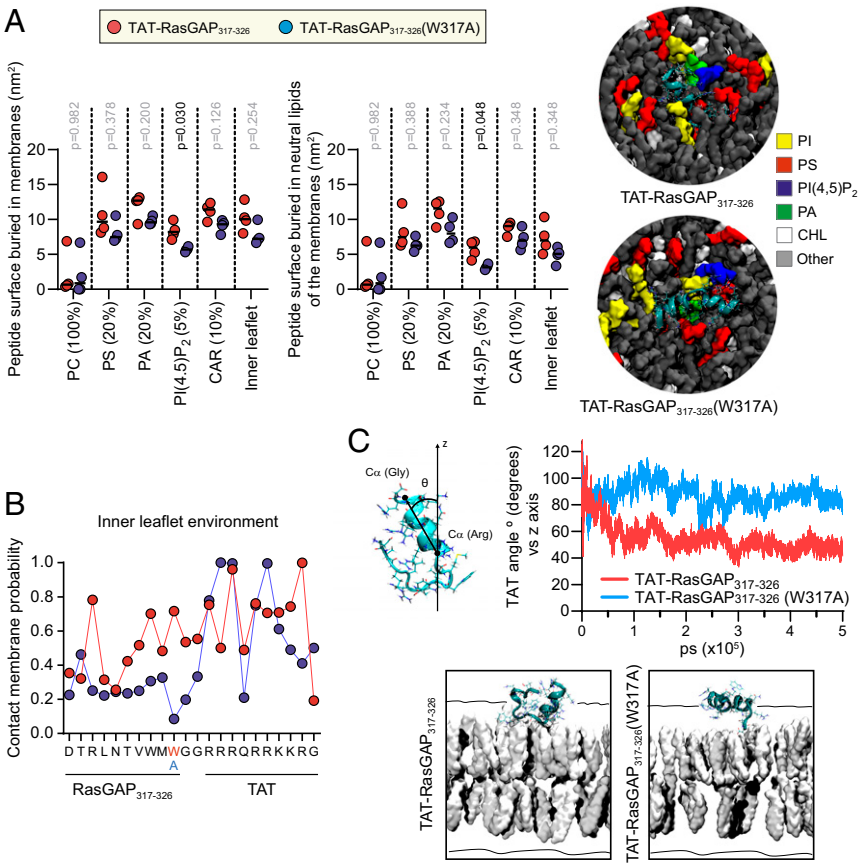


**Fig. 7.** The W317A mutation affects the structure of TAT-RasGAP$_{317–326}$ and its ability to interact with membranes. (*A*) The propensity of TAT-RasGAP$_{317–326}$ and its W317A mutant to penetrate membranes with the indicated compositions (*SI Appendix*, Table S3) was analyzed by computing the buried surface with GROMACS tools and homemade scripts. The graph on the *Left* presents the surface of the peptides buried within all of the lipids of the contacting leaflet, while the graph on the *Right* considers only the surface of the peptides buried within neutral lipids of the membrane (e.g., PC). Paired *t* tests were used to assess statistical significance. The images to the *Right* of the graphs are snapshots of the interaction of TAT-RasGAP$_{317–326}$ or its W317A mutant with inner-leaflet–like membranes. (*B*) Probability of the individual residues within TAT-RasGAP$_{317–326}$ or its W317A mutant to establish contact with the inner-leaflet composition membrane. Only the last 50 ns of the 500-ns simulation runs were considered for this analysis. The results correspond to the median of four separate simulations. (*C*) In the image shown on the *Left*, θ corresponds to the angle between the normal to the membrane (Z) and the long axis of the helically folded TAT segment (Cα [Arg]-Cα[Gly] vector). The graph shows the median change of this angle in four separated simulations of TAT-RasGAP$_{317–326}$ and its W317A mutant in inner-leaflet–like membranes. The images below depict simulation snapshots of peptide interaction with the inner-leaflet composition membrane (*SI Appendix*, Table S3). Only the peptides and cholesterol molecules are shown, and thin lines represent the limit of phospholipid heads.

*Appendix*, Fig. S1) (13). Once in the cytoplasm, the peptide targets anionic phospholipids, such as PI(4,5)$P_2$ and PS, that are enriched in the inner layer of the plasma membrane. This interaction destabilizes the plasma membrane apparently in a detergent-like manner, compromising its integrity and ultimately leading to a necrotic type of cell death. In addition, this study also gives an explanation of why the substitution of the tryptophan at position 317 for an alanine residue in TAT-RasGAP$_{317–326}$ profoundly decreases the ability of the peptide to enter and kill cells.

Distinct uptake efficiencies between the wild-type and the mutant peptides are not explained by differences in peptide–lipid interaction since both peptides interact similarly —and rather inefficaciously—with outer membrane lipids (Fig. 1). Rather, it may be the higher ability of the wild-type peptide to promote negative curvature in zwitterionic membranes such as the outer membrane that could facilitate peptide entry (*SI Appendix*, Fig. S10).

Once inside cells, the killing ability of the peptides is modulated by peptide-membrane interplay. TAT-RasGAP$_{317–326}$, but not the W317A mutant, efficiently interacts with anionic lipids such as PI(4,5)$P_2$, PS, or cardiolipin. This cannot be explained by global differences in electrostatic interactions between the peptides and the membrane as both wild-type and mutant peptides carry the same net positive charges (+9). The two peptides do not share the same secondary structures, however, the W317A substitution strongly favoring α-helix formation in the RasGAP moiety. This is likely an important determinant for the membranolytic activity of TAT-RasGAP$_{317–326}$. For example, compared to the W317A mutant, the less structured wild-type peptide "attacks" membranes with a sharper angle allowing deeper insertion into the lipid core. In addition, in comparison to alanine, a tryptophan residue at position 317 increases the ability of the surrounding amino acids to move closer to lipids (Fig. 7). Disruption of α-helix formation in the RasGAP moiety is not a unique property of tryptophan, but rather of aromatic amino acids since a phenylalanine residue can be substituted for tryptophan at position 317 without affecting the peptide's activity (*SI Appendix*, Fig. S11). Finally, in the presence of anionic lipids, wild-type TAT-RasGAP$_{317–326}$ gains the ability to induce positive membrane curvature, while the mutant peptide behaves identically in all membranes tested (*SI Appendix*, Fig. S10). This can be interpreted as the wild-type peptide binding more avidly to anionic membranes compared to the mutant peptide, facilitating membrane disruption. The "rigidity" of the W317A peptide weakens the interactions with lipid membranes containing

anionic lipids, flattens the angle of action, and diminishes peptide–lipid interaction. This could mechanistically explain the reduced biological activity of the W317A mutant.

TAT-RasGAP$_{317–326}$ displays binding preferences for certain, but not all, anionic lipids. For example, the peptide binds phosphoinositide biphosphate better than phosphoinositide mono- or triphosphate. In addition, TAT-RasGAP$_{317–326}$ membrane-destabilizing activity is affected differently by negatively charged lipids. For example, cardiolipin vesicles, which allow efficient TAT-RasGAP$_{317–326}$ binding, are not well permeabilized. As mentioned above, these phenomena cannot simply be explained by electrostatic interactions but rather, as suggested by others (18), by the lipid and membrane topology, modulating peptide–lipid binding and peptide membranolytic activity.

Plasma membrane damage induced by TAT-RasGAP$_{317–326}$ can be repaired, at least to a certain extent, by the ESCRT machinery as the inhibition of the latter sensitizes cells to the peptide (Fig. 5). This suggests that cells tolerate a certain amount of TAT-RasGAP$_{317–326}$–induced plasma membrane damage because they can engage membrane repair pathways such as the one triggered by the ESCRT machinery. Only when the membrane repair capacity of the cells is overwhelmed by high enough concentrations of cytosolic TAT-RasGAP$_{317–326}$ will cells undergo necrosis. Since TAT-RasGAP$_{317–326}$ induces a nonregulated necrotic type of death, cells do not have the possibility of developing a resistance based on mutations in elements of programmed cell death pathways. However, they might still acquire resistance through altering membrane lipid composition, mutations of genes participating in the making of specific elements of the plasma membrane, or up-regulating the cell's ability to repair its plasma membrane.

A number of cationic peptides have shown interesting anticancer properties, including their ability to deliver drugs into cells, and through intrinsic antimetastatic, antiangiogenic, and apoptosis potentiating properties (17, 28). However, only a limited subset of these peptides display substantial membranolytic activities through interaction with phosphoinositides. That is the case of some plant defensins, such as NaD1 (*Nicotiana alata Defensin 1*) or TPP3, which disrupt the plasma membrane of cells through interaction with phosphoinositides such as PI(4,5)$P_2$ (29–31) in a mechanism that appears similar to the one described here for TAT-RasGAP$_{317–326}$. However, there are differences in terms of lipid preferences between NaD1, TPP3, and TAT-RasGAP$_{317–326}$. NaD1 is promiscuous in its ability to bind phosphoinositides. In contrast, TPP3 interacts only with PI(4,5)$P_2$. TAT-RasGAP$_{317–326}$ has an intermediate selectivity for phosphoinositides, being able to bind more efficiently all of the tested phosphatidylinositol bisphosphate. The cell translocation mechanism of TAT-RasGAP$_{317–326}$ has been characterized in detail (13), but how NAD1 and TPP3 enter cells is still incompletely understood.

The potential clinical applications of TAT-RasGAP$_{317–326}$ are likely restricted to topical or on-target usage as the biodistribution and bioavailability of TAT-RasGAP$_{317–326}$ is suboptimal for systemic applications (7, 9). The present characterization of the mode-of-action allowing this peptide to permeabilize the membrane of cancer cells may facilitate the search for small molecules mimicking the peptide's structure and carrying the peptide's killing activity.

## Materials and Methods

For information on reagents, chemicals, immunoblotting, GUV and MLV generation, in silico modeling, CD, ssNMR, electron microscopy, confocal microscopy, and experimental model systems, see *SI Appendix*. The lipids used in this study are described in *SI Appendix*, Table S1. The plasma membrane composition considered for our experiments is presented in *SI Appendix*, Table S2. The composition of the membranes used in in silico simulations is shown in *SI Appendix*, Table S3. The tested peptides are listed in *SI Appendix*, Table S4. Plasma membrane depolarization was induced by 100 mM extracellular KCl. Fluorescein isothiocyanate (FITC)-labeled peptide binding to cells and cellular uptake were measured by flow cytometry in the presence or in the absence of the trypan blue fluorescent quencher. Cytosolic access of peptides was assessed by confocal imaging. Phosphatidylserine cellular levels were measured with Annexin-V in permeabilized cells. Cell death was assessed by colony formation assays or by flow cytometry based on PI or DAPI staining or changes in cell complexity. PI(4,5)$P_2$ depletion was performed using a rapamycin-triggered plasma membrane recruitment of a lipid phosphatase.

**Data Availability.** All study data are included in the article and supporting information.

**ACKNOWLEDGMENTS.** We thank Navin Gopaldass and Andreas Mayer (Department of Biochemistry, University of Lausanne) for their technical support in liposome preparation and Dora Hancz and Petr Broz (Department of Biochemistry, University of Lausanne) for providing the HeLa cell lines expressing the dominant negative CHMP3$_{1–179}$ and VPS4A$^{E228Q}$ mutants. We thank Yannick Krempp and Luigi Bozzo (Cellular Imaging Facility, University of Lausanne) for their support in image acquisition. We acknowledge support from France BioImaging (Grant ANR10INSB04). This work was supported by a grant from the Swiss National Supercomputing Centre.

1. R. Valentin, S. Grabow, M. S. Davids, The rise of apoptosis: Targeting apoptosis in hematologic malignancies. *Blood* **132**, 1248–1264 (2018).
2. K. Fernald, M. Kurokawa, Evading apoptosis in cancer. *Trends Cell Biol.* **23**, 620–633 (2013).
3. D. Hanahan, R. A. Weinberg, Hallmarks of cancer: The next generation. *Cell* **144**, 646–674 (2011).
4. D. Michod, J. Y. Yang, J. Chen, C. Bonny, C. Widmann, A RasGAP-derived cell permeable peptide potently enhances genotoxin-induced cytotoxicity in tumor cells. *Oncogene* **23**, 8971–8978 (2004).
5. D. Barras, G. Lorusso, C. Rüegg, C. Widmann, Inhibition of cell migration and invasion mediated by the TAT-RasGAP$_{317-326}$ peptide requires the DLC1 tumor suppressor. *Oncogene* **33**, 5163–5172 (2014).
6. N. Chevalier, N. Gross, C. Widmann, Assessment of the chemosensitizing activity of TAT-RasGAP$_{317-326}$ in childhood cancers. *PLoS One* **10**, e0120487 (2015).
7. M. Heulot *et al*., The anticancer peptide TAT-RasGAP$_{317-326}$ exerts broad antimicrobial activity. *Front. Microbiol.* **8**, 994 (2017).
8. P. Tsoutsou *et al*., TAT-RasGAP$_{317-326}$ enhances radiosensitivity of human carcinoma cell lines in vitro and in vivo through promotion of delayed mitotic cell death. *Radiat. Res.* **187**, 562–569 (2017).
9. D. Michod *et al*., Effect of RasGAP N2 fragment-derived peptide on tumor growth in mice. *J. Natl. Cancer Inst.* **101**, 828–832 (2009).
10. D. Sarko *et al*., The pharmacokinetics of cell-penetrating peptides. *Mol. Pharm.* **7**, 2224–2231 (2010).
11. D. Barras *et al*., A WXW motif is required for the anticancer activity of the TAT-RasGAP$_{317-326}$ peptide. *J. Biol. Chem.* **289**, 23701–23711 (2014).
12. M. Heulot *et al*., The TAT-RasGAP$_{317-326}$ anti-cancer peptide can kill in a caspase-, apoptosis-, and necroptosis-independent manner. *Oncotarget* **7**, 64342–64359 (2016).
13. E. Trofimenko *et al*, Potassium channels, megapolarization, and water pore formation are key determinants for cationic cell-penetrating peptide translocation into cells. https://doi.org/10.1101/2020.02.25.963017 (26 February 2020).
14. J. B. Rothbard, T. C. Jessop, R. S. Lewis, B. A. Murray, P. A. Wender, Role of membrane potential and hydrogen bonding in the mechanism of translocation of guanidinium-rich peptides into cells. *J. Am. Chem. Soc.* **126**, 9506–9507 (2004).
15. D. Gaspar, A. S. Veiga, M. A. R. B. Castanho, From antimicrobial to anticancer peptides. A review. *Front. Microbiol.* **4**, 294 (2013).
16. F. Schweizer, Cationic amphiphilic peptides with cancer-selective toxicity. *Eur. J. Pharmacol.* **625**, 190–194 (2009).
17. B. Deslouches, Y. P. Di, Antimicrobial peptides with selective antitumor mechanisms: Prospect for anticancer applications. *Oncotarget* **8**, 46635–46651 (2017).
18. D. J. Paterson, M. Tassieri, J. Reboud, R. Wilson, J. M. Cooper, Lipid topology and electrostatic interactions underpin lytic activity of linear cationic antimicrobial peptides in membranes. *Proc. Natl. Acad. Sci. U.S.A.* **114**, E8324–E8332 (2017).
19. A. J. Jimenez *et al*., ESCRT machinery is required for plasma membrane repair. *Science* **343**, 1247136 (2014).
20. S. Rühl *et al*., ESCRT-dependent membrane repair negatively regulates pyroptosis downstream of GSDMD activation. *Science* **362**, 956–960 (2018).
21. L. M. Reid, C. S. Verma, J. W. Essex, The role of molecular simulations in understanding the mechanisms of cell-penetrating peptides. *Drug Discov. Today* **24**, 1821–1835 (2019).
22. B. Hernández *et al*., Octreotide used for probing the type-II′ β-turn CD and Raman markers. *J. Phys. Chem. B* **116**, 9337–9345 (2012).
23. M. Bagheri, S. Keller, M. Dathe, Interaction of W-substituted analogs of cyclo-RRRWFW with bacterial lipopolysaccharides: The role of the aromatic cluster in antimicrobial activity. *Antimicrob. Agents Chemother.* **55**, 788–797 (2011).

24. V. V. Andrushchenko, H. J. Vogel, E. J. Prenner, Solvent-dependent structure of two tryptophan-rich antimicrobial peptides and their analogs studied by FTIR and CD spectroscopy. *Biochim. Biophys. Acta* **1758**, 1596–1608 (2006).
25. C. Byrne, M. Belnou, E.-E. Baulieu, O. Lequin, Y. Jacquot, Electronic circular dichroism and nuclear magnetic resonance studies of peptides derived from the FKBP52-interacting β-turn of the hERα ligand-binding domain. *Pept. Sci. (Hoboken)* **111**, e24113 (2019).
26. T. Murayama *et al*., Loosening of lipid packing promotes oligoarginine entry into cells. *Angew. Chem. Int. Ed. Engl.* **56**, 7644–7647 (2017).
27. S. Afonin *et al*., The cell-penetrating peptide TAT(48-60) induces a non-lamellar phase in DMPC membranes. *Chemphyschem* **7**, 2134–2142 (2006).
28. D. Raucher, J. S. Ryu, Cell-penetrating peptides: Strategies for anticancer treatment. *Trends Mol. Med.* **21**, 560–570 (2015).
29. A. A. Baxter, I. K. Poon, M. D. Hulett, The plant defensin NaD1 induces tumor cell death via a non-apoptotic, membranolytic process. *Cell Death Discov.* **3**, 16102 (2017).
30. A. A. Baxter *et al*., The tomato defensin TPP3 binds phosphatidylinositol (4,5)-bisphosphate via a conserved dimeric cationic grip conformation to mediate cell lysis. *Mol. Cell. Biol.* **35**, 1964–1978 (2015).
31. I. Kh. Poon *et al*., Phosphoinositide-mediated oligomerization of a defensin induces cell lysis. *eLife* **3**, e01808 (2014).
32. Y. Wang, F. Wang, R. Wang, P. Zhao, Q. Xia, 2A self-cleaving peptide-based multi-gene expression system in the silkworm Bombyx mori. *Sci. Rep.* **5**, 16273 (2015).
33. B.-C. Suh, T. Inoue, T. Meyer, B. Hille, Rapid chemically induced changes of PtdIns(4,5) $P_2$ gate KCNQ ion channels. *Science* **314**, 1454–1457 (2006).
34. D. Raucher *et al*., Phosphatidylinositol 4,5-bisphosphate functions as a second messenger that regulates cytoskeleton-plasma membrane adhesion. *Cell* **100**, 221–228 (2000).
35. D. J. Tóth *et al*., Acute depletion of plasma membrane phosphatidylinositol 4,5-bisphosphate impairs specific steps in endocytosis of the G-protein-coupled receptor. *J. Cell Sci.* **125**, 2185–2197 (2012).